Polymer conversion into amorphous ceramics by ion irradiation

E. Z. KURMAEV
*Institute of Metal Physics, Russian Academy of Sciences-Ural Division,
620219 Yekaterinburg GSP-170, Russia*

A. MOEWES
*Department of Physics and Engineering Physics, University of Saskatchewan,
Saskatoon, Canada*
E-mail: moewes@usask.ca

J.-C. PIVIN
*Centre de Spectrométrie Nucléaire et de Spectrométrie de Masse, IN2P3-CNRS,
Bâtiment 108, 91405 Orsay Campus, France*

M. BACH
Universitat Osnabrück, Fachbereich Physik, D-49069 Osnabrück, Germany

K. ENDO, T. IDA, S. SHIMADA
*Department of Chemistry, Faculty of Science, Kanazawa University,
Kakuma-machi, Kanazawa, 920-1192 Japan*

M. NEUMANN
Universitat Osnabrück, Fachbereich Physik, D-49069 Osnabrück, Germany

S. N. SHAMIN
*Institute of Metal Physics, Russian Academy of Sciences-Ural Division,
620219 Yekaterinburg GSP-170, Russia*

D. L. EDERER
Department of Physics, Tulane University, New Orleans, LA 70118, USA

M. IWAMI
Research Laboratory for Surface Science, Okayama University, Okayama 700-8530, Japan

We present results of X-ray fluorescence measurements (carbon $K\alpha$ and Si $L_{2,3}$) of methylhydroxylsiloxane and phenylmethylhydroxylsiloxane films. The films are converted into amorphous ceramics by irradiation with 500 keV C and 3 MeV Au ions. Changes in the composition (O/Si ratio) of some polysiloxane films are found when treated with ion irradiation. It is shown that ion irradiation induces a segregation of carbon atoms from methyl groups into diamond-like clusters whereas carbon atoms from phenyl groups maintain their sp^2 configuration. © *2002 Kluwer Academic Publishers*

1. Introduction

Recently it has been shown that ion irradiation of polysiloxane films converts them into amorphous ceramics (SiC, SiOC) with increased hardness, oxidation resistance and thermal stability [1]. Such treatment is found to be more efficient than polymer pyrolysis [2], because it provides a more complete release of hydrogen [3–4]. The composition and structure of various irradiated polysiloxane films have been studied by means of Rutherford backscattering, elastic recoil detection analysis, nuclear reaction analysis, Raman, and Fourier transform-infrared spectroscopies [1]. Based on these measurements, increased hardness and thermo chemical stability of irradiated polysiloxane coatings were attributed to a segregation of carbon atoms into diamond-like clusters.

In order to confirm these conclusions, we have performed X-ray fluorescence measurements of irradiated methylhydroxylsiloxane and phenylmethylhydroxyl-siloxane films. Earlier we applied this technique to study the chemical changes induced by irradiation in polycarbosilane [5], polyetherosulphone [6] and phenyltriethoxysilane [7] films. We found changes in the O/Si ratio after ion irradiation. It has been concluded that during irradiation carbon atoms of phenyl groups tend to retain their sp^2 configuration whereas carbon atoms from the methyl groups form diamond-like clusters causing the increased high hardness of ceramic films.

TABLE I Overview on treatment of the samples and the film thickness

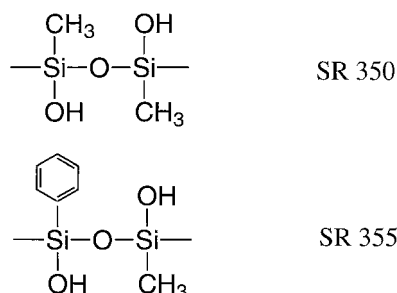| Sample	Treatment	Thickness
SR 350	Unirradiated	650 nm
SR 350	2.5×10^{14} Au (3 MeV)	650 nm
SR 350	1.1×10^{15} Au (3 MeV)	650 nm
SR 350	2.5×10^{15} Au (3 MeV)	650 nm
SR 355	Unirradiated	1080 nm
SR 355	5×10^{14} Au (3 MeV)	720 nm
SR 355	2.5×10^{15} Au (3 MeV)	720 nm
SR 355	5.5×10^{14} C (500 keV)	700 nm
SR 355	Unirradiated + 1000°C	575 nm
SR 355	10^{16} C (500 keV) + 1000°C	700 nm

Figure 1 Chemical structure of the samples: methylhydroxylsiloxane (SR 350) and phenylmethylhydroxylsiloxane (SR 355).

2. Experimental

SiOC films with thickness of about 650–1080 nm have been prepared from ethanol solutions of two different pre-ceramic polymers: methylhydroxyl-siloxane (SR 350) and phenylmethylhydroxylsiloxane (SR 355). Their chemical structure is shown in Fig. 1. The films were irradiated at room temperature with 500 keV C or 3 MeV Au ions (see Table I) provided by the ARAMIS accelerator of CSNSM [8]. The ion power was limited to 0.1 Wcm^{-2} so as to avoid a significant heating of the samples during irradiation.

The carbon Kα (2p $\rightarrow$ 1s transition) and silicon L$_{2,3}$ (3s3d $\rightarrow$ 2p transition) X-ray emission spectra (XES) were measured at Beamline 8.0 of the Advanced Light Source (ALS) at Lawrence Berkeley National Laboratory (LBNL, Berkeley) employing the University of Tennessee at Knoxville's soft X-ray fluorescence (SXF) endstation [9]. Photons with energies of 310 eV, well above the carbon K-absorption edge, 560 eV above the oxygen K-absorption edge and 110 eV, well above the silicon L absorption edge, were delivered to the endstation via the beamline's undulator insertion device and spherical grating monochromator. The carbon and oxygen Kα were obtained with a 600 lines/mm, 10 meter radius grating and energy resolution of about 0.4–0.5 eV. The silicon L$_{2,3}$ XES were measured with a 1500 lines/mm, 5 meter radius grating and energy resolution of about 0.3 eV. The energies of the carbon Kα and silicon L$_{2,3}$ XES were calibrated with reference spectra of highly oriented pyrolytic graphite (HOPG) and crystalline silicon.

The x-ray photoelectron spectroscopy (XPS) measurements were taken with a PHI 5600 ci ESCA spectrometer using monochromatized aluminum Kα radiation with 0.3 eV FWHM. The energy resolution of the analyzer was 1.5% of the pass energy. We es-

timated that the energy resolution of the spectrometer is about 0.35 eV for XPS measurements. All measurements were performed at room temperature. The XPS spectra were calibrated using the Au 4f$_{7/2}$ signal from a gold foil sample. The binding energy for Au 4f$_{7/2}$ electrons is 84.0 eV.

3. Results and discussion

In the x-ray emission process the absorption of the incoming photon leads to an electronic transition from the initial state to the excited state (intermediate state). The excitation is followed by the decay of the excited state to the final state and a photon is emitted. Soft X-ray emission measurements provide chemical information in the form of local density of states distribution of certain symmetries allowed by the dipole selection rules and the localization of core-level states. Therefore, using carbon and oxygen Kα XES (2p $\rightarrow$ 1s transition) we probe the distribution of 2p-occupied states and Si L$_{2,3}$ XES (3s3d $\rightarrow$ 2p transition) provides information about Si 3s3d occupied states.

3.1. Carbon Kα X-ray emission spectra

Fig. 2a shows C Kα XES of SR 350 and SR 355 unirradiated films. Carbon Kα XES of SR 355 exhibits a three-peak structure, which resembles that of benzene [10] because most carbon atoms belong to the phenyl groups (see Fig. 1). On the other hand, C Kα XES of SR 350 has a less pronounced fine structure and reflects the distribution of C 2p-occupied orbitals of methyl groups and C–Si bonds.
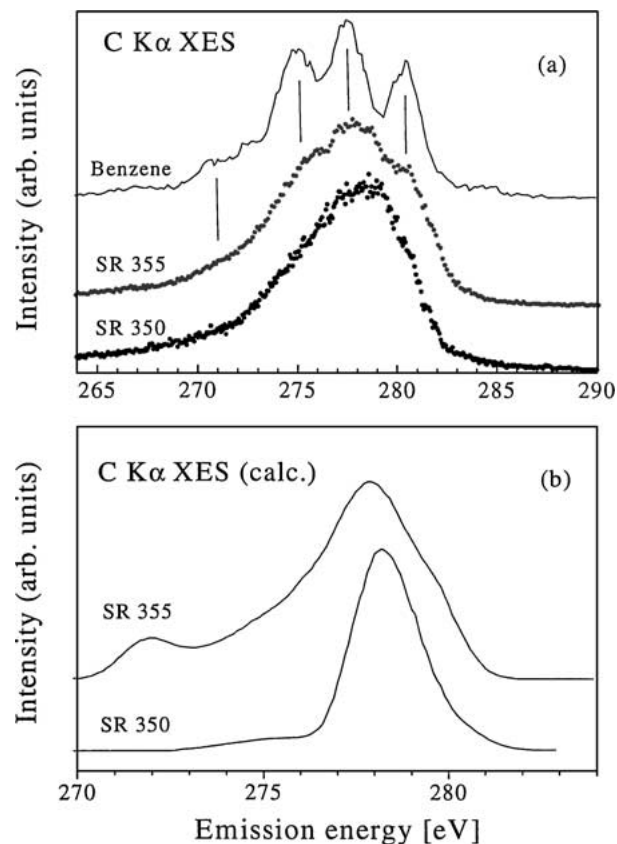
Figure 2 Carbon Kα x-ray emission spectra (XES) of measured (a) and calculated (b) unirradiated SR 350 and SR 355. For comparison the measured emission spectrum of Benzene is shown.

To compare our experimental spectra with theory we have carried out calculations of Carbon Kα emission spectra of SR 350 and SR 355 within the molecular models using a deMon density functional theory (DFT) program [11, 12]. Optimized Cartesian coordinates from the semi-empirical AM1 method (version 6.0) have been used for the geometry of molecules [13]. The deMon calculations were performed using B88/P86 exchange-correlation potential obtained from Becke's 1988 exchange functional [14] and Perdew's 1986 correlation functional [15]. The intensity of C Kα XES peaks was obtained by summing populations (the squares of the linear combination of atomic orbitals (LCAO) coefficients, $|C_{j[2p(A)]_l}|^2$,) of the atomic orbitals $\chi_{2p(A)}(r)$ centered at the given carbon atoms, where $l = x$, y, and z. We approximated the populations as obtained from the deMon DFT calculations of the model molecules for SR 350 and 355 with an STO-3G basis set. Each peak in the theoretical XES spectrum is also broadened by a Gaussian line shape function, with the same weight and full-width at half-maximum (FWHM = 1.3 eV) as the experimental spectrum.

Fig. 2b displays calculations of the measured spectra of SR 350 and SR 355. Apparently the C Kα XES of SR 355 is broader and consists of more spectral features than that of SR 350. According to our calculation, the p_π (C 2p—C 2p) bonding orbitals of phenyl groups contribute predominantly to the C Kα XES emission of SR 355. In the case of SR 350 the situation is different and both p_σ (C 2p—Si 3p) and p_π (C 2p—Si 3s) bonding orbitals of Si—C bonds form the intensity distribution of C Kα XES. In general good agreement between experimental and calculated spectra is obtained although the calculated C Kα XES of SR 355 do not reproduce all the fine structure of the experimental data. The peaks exhibited at about 268 and 272 eV in the calculation for sample SR 355 is due to p_σ bonding orbitals of C 2p—Si 3s bonds and are not found in the experimental data.

Ion irradiation induces noticeable changes in the intensity distribution of C Kα XES of SR 355 (Fig. 3a). An increase in broadening of the three-peak structure with increasing fluence is observed. The C Kα XES of strongly irradiated SR 355 film becomes similar to the spectrum of amorphous carbon film (a-C) [16] which consists of 80% of sp^2 bonded carbon and is quite different from the spectrum of diamond-like film (IBAM219). This can be attributed to a release of hydrogen atoms from the phenyl rings induced by ion irradiation.

The annealing of SR 355 polysiloxane films for 1 hr at 1000°C under a vacuum of 10^{-6} Torr modifies the fine structure of C Kα XES making it more similar to that of HOPG (Fig. 4). This could be due to segregation of sp^2-clusters of carbon atoms induced by annealing which would agree with previous conclusions from Raman measurements [1].

Fig. 3b shows C Kα XES of irradiated SR 350 films. It is necessary to point out that in this case we also observe changes in the spectral profile of C Kα XES with increasing ion fluence. One can note that irradiation induces the appearance of a high-energy feature around 280.5 eV. The comparison of C Kα XES of SR 350 film irradiated with 2.5×10^{14} cm^{-2} and spectrum of

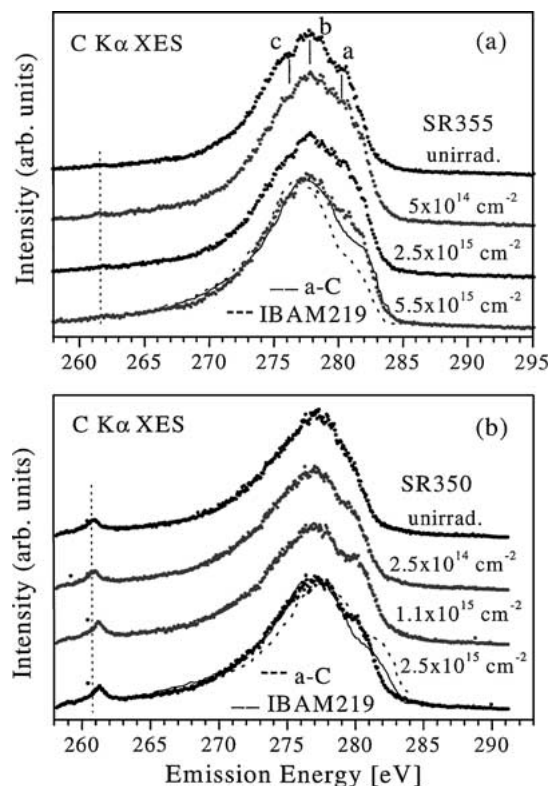*Figure 3* Carbon Kα x-ray emission spectra of irradiated SR 355 (a) and SR 350 (b) films irradiated with different fluence of Au ions. For dosage and film thicknesses see Table I. For comparison the spectra of reference samples of amorphous carbon (a-C) and diamond-like film (IBAM219) are shown.
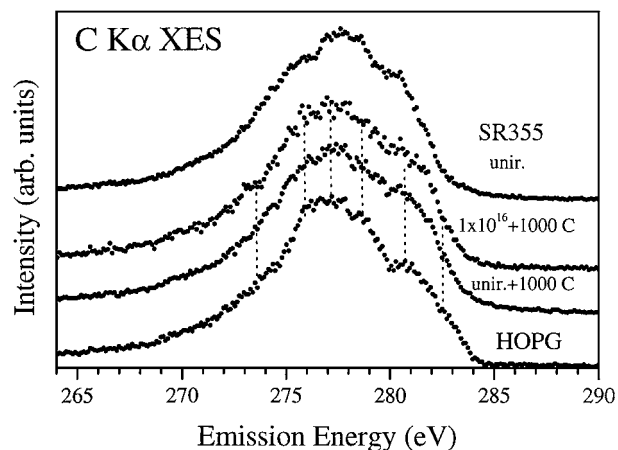

Figure 4 C Kα XES of annealed SR 355 films with reference spectrum of HOPG.

diamond-like film taken from Ref. [16] shows a good agreement. On the other hand, we note that C Kα XES of heavily irradiated SR 350 film is different from that of amorphous carbon. Therefore, we can conclude that ion irradiation of SR 350 films at low fluences induces a segregation of carbon atoms from methyl groups into diamond-like clusters.

3.2. Silicon L$_{2,3}$ X-ray emission spectra
Si L$_{2,3}$ XES of irradiated and annealed SR 355 and SR 350 films are presented in Fig. 5a and b.) According to our deMon DFT calculations, the fine structure of Si L$_{2,3}$ XES consists of two peaks labeled *A* and *B*, which have main contributions from Si—O bonds and some contributions from Si—C bonds and their ratio is found
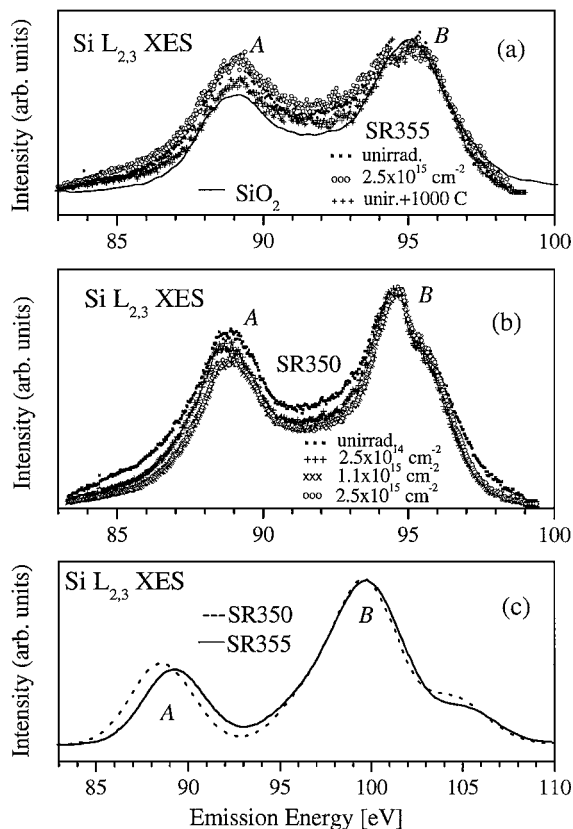
Figure 5 Si L$_{2,3}$ XES of unirradiated, irradiated and annealed SR 355 (a) and SR 350 (b) films and calculated Si L$_{2,3}$ XES of SR 355 and SR 350 (c). For comparison the spectra are normalized to the same peak height of peak B.

Figure 6 (a) Comparison of x-ray photoelectron valence band spectrum with the C Kα, O Kα and Si L$_{2,3}$ XES of SR 350 on the common binding energy scale. The calculated x-ray photoelectron valence band spectra (b) of SR 350 and SR 355 are very similar.

to be the same (about 0.40) for both SR 350 and SR 355 (Fig. 5c). However, as seen in Fig. 5a and b, this ratio is different in experimental spectra of unirradiated films: 0.75 for unirradiated SR 350 and 0.90 for SR 355. This intensity ratio is sensitive to the O/Si composition ratio and varies from 0.66 for SiO$_2$ to 0.86 for SiO$_{1.7}$ [17]. Therefore it is possible to estimate the resistance to oxidation of irradiated and annealed polysiloxane films from Si L$_{2,3}$ XES measurements.

We have not found any changes in the intensity ratio of peaks A to B in Si L$_{2,3}$ XES for SR 355 films with irradiation up to a fluence of 2.5×10^{15} cm^{-2} (Fig. 5a) and can therefore conclude that these irradiated films have high resistance to oxidation. On the other hand, the ion irradiation of SR 350 films up to 1×10^{15} cm^{-2} reduces the intensity ratio A/B of Si L$_{2,3}$ XES (see Fig. 5b) which we attribute to an increase in O/Si composition ratio. This could be due to an increase of bonds cross-linking, which is easier in SR 350 than in SR 355 because of the smaller volume of CH$_3$ group.

For both films annealing at 1000°C reduces the ratio of peaks A to B (see Fig. 5a) indicating that the O/Si ratio becomes closer to the one found for SiO$_2$. This is in agreement with previous measurements of areal densities and thicknesses according to which the carbon concentration annealed polysiloxane films decreases to about 40–45% of the original concentration [1] thus providing the possibility that they are oxidized.

The conclusion we come to regarding the higher resistance of irradiated SR 355 films to the oxidation deduced from an analysis of Si L$_{2,3}$ XES is supported by
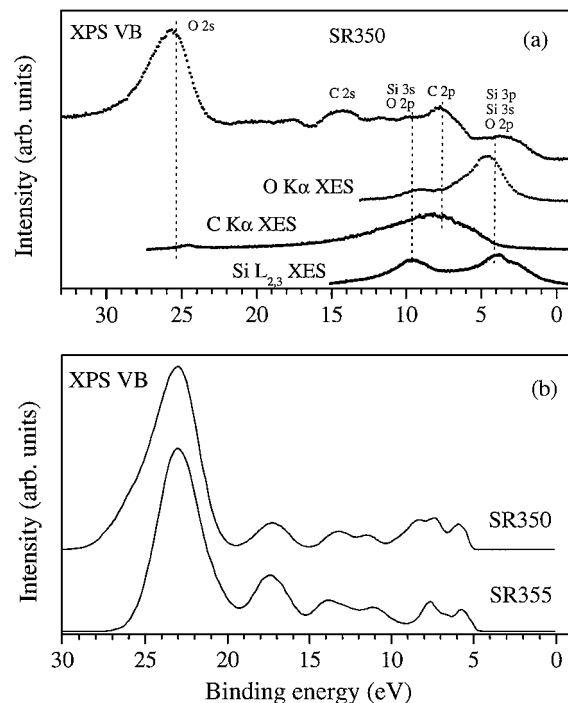
the C Kα XES data displayed in Fig. 3a and b. The low-energy sub-band centered at about 261 eV shows much higher intensity for SR 350 than for SR 355 films. According to our deMon DFT calculations and comparison of C Kα XES and XPS valence band (VB) (Fig. 6a) this sub-band is due to C 2p–O 2s hybridization and can be used to estimate the amount of chemically bonded oxygen. Therefore, the low intensity of this sub-band is due to a high resistance of irradiated SR 355 films to oxidation.

3.3. X-ray photoelectron valence band spectra

The calculated XPS VB spectra of SR 350 and SR 355 (see Fig. 6b) are very similar. For this reason why we have measured only XPS VB of SR 350 (Fig. 6a). The XPS VB probes the total density of states in the valence band and gives a general picture of the distribution of all occupied electronic states. Two parts contribute to the fundamental structure of XPS VB of SR 350 and SR 355. The spectral structure in the region of binding energies from 12 to 30 eV can be attributed to atomic-like C 2s and O 2s-states taking into account atomic photo ionization cross-sections for aluminum Kα radiation [18]. In the region of binding energies from 0 to 12 eV one can expect to observe XPS VB peaks of Si 3p3s, C 2p and O 2p-states. These peaks can be correctly assigned by the deMon DFT calculations and the comparison of XPS VB with C Kα and Si L$_{2,3}$ XES on the common binding energy scale.

We calculated XPS VBs of SR 350 and SR 355 based on our deMon DFT data (see Fig. 6b). The intensities of the peaks follow the oxygen, carbon and silicon content of the polymers weighted with the atomic photo ionization cross-sections [18]. For calculation details

TABLE II Observed peaks, vertical ionization potential (VIP), main photoelectron ionization cross-section of the atomic orbitals (AO PICS), orbital nature and the functional group (FG) for the valence band photoelectron spectrum of SR 350 (the shift between observed and calculated vertical ionization potentials (VIPs) = 3.5 eV)

Peak (eV)	VIP (eV)	Main AO PICS	Orbital nature	FG
25.7	25.69–22.65	O 2s(0.9), Si 3s(0.1)	s_σ (O 2s-Si 3s)-B	O—Si
17.6, 14.2	17.77, 16.85	C 2s(0.7), Si 3s(0.3)	s_σ (C 2s-Si 3s)-B	C—Si
11.7, 9.9	13.75, 12.96, 11.71	O 2p(0.6), Si 3s(0.4)	p_σ (O 2p-Si 3s)-B	O—Si
7.8	9.0–7.4	O 2p(0.8), Si 3p(0.2)	p_π (O 2p-Si 3p)-B	O—Si
3.7	6.57–5.55	O 2p	p_π (lone pair)-NB	—O—

see Ref. 7. The calculated peaks (vertical ionization potentials, VIP) are compared with the experimental peaks in Table II. Table II lists also the main atomic orbitals (AOs) and the functional groups of these spectra. The most intense peak of the measured spectrum of SR 350 located around 25.7 eV corresponds to ionization of s_σ (O 2s—Si 3s) bonding orbitals that are related to oxygen-silicon bonds. The next group of XPS VB peaks situated around 17.6–14.2 eV can be attributed to s_σ (C 2s—Si 3s) bonding orbitals which are formed by carbon-silicon bonds. The peaks at 11.7 and 9.9 eV are due to p_σ (O 2p—Si 3s) bonding orbitals and the peak at 7.8 eV to p_σ (C 2p—Si 3s3p) is due to bonding orbitals. According to the calculations, non-bonding orbitals of oxygen p_π (lone pair) are concentrated at the top of the valence band (around 3.7 eV).

In order to verify this assignment, we have compared XPS VB with carbon and oxygen Kα and silicon L$_{2,3}$ XES of SR 350 (which probe the distribution of the occupied C 2p, O 2p and Si 3s3d-states in the valence band, respectively) (see Fig. 6a). The XES are converted to the common binding energy scale using our XPS measurements of core level binding energies. This comparison supports the interpretation of XPS VB given above, based on our deMon DFT calculations.

4. Conclusion
In summary we have performed a full study of the electronic structure of unirradiated and irradiated methylhydroxylsiloxane and phenylmethylhydroxylsiloxane films by means of X-ray emission and photoelectron spectroscopy and deMon DFT calculations. We have found that conversion of polysiloxane films into ceramics induced by ion irradiation goes along with an increase of the O—Si ratio and of the O—C bonding due to the release of H and the formation of dangling bonds. It is shown that carbon atoms from phenyl groups retain their sp^2 hybridization state whereas atoms from methyl groups segregate into diamond-like clusters providing the increased hardness of ceramic films.

References
1. J. C. PIVIN and P. COLOMBO, *J. Mater. Sci.* **32** (1997) 6163.
2. M. HARRIS, T. M. CHAUDHARY, L. DRZAL and R. M. LANE, *Mater. Sci. Eng.* A **195** (1995) 223.
3. J. C. PIVIN and P. COLOMBO, *Nucl. Instrum. Methods* B **120** (1996) 262.
4. *Idem.*, *J. Mater. Sci.* **32** (1997) 6175.
5. R. P. WINARSKI, D. L. EDERER, J.-C. PIVIN, E. Z. KURMAEV, S. N. SHAMIN, A. MOEWES, G. S. CHANG, C. N. WHANG, K. ENDO and T. IDA, *Nucl. Instrum. Methods* B **145** (1998) 401.
6. E. Z. KURMAEV, R. P. WINARSKI, K. ENDO, T. IDA, A. MOEWES, D. L. EDERER, J.-C. PIVIN, S. N. SHAMIN, V. A. TROFIMOVA and YU. M. YARMOSHENKO, *ibid.* B **155** (1999) 431.
7. E. Z. KURMAEV, A. MOEWES, M. KRIETMEYER, K. ENDO, T. IDA, S. SHIMADA, R. P. WINARSKI, M. NEUMANN, S. N. SHAMIN and D. L. EDERER, *Phys. Rev.* B **60** (1999) 15100.
8. E. COTTEREAU, J. CAMPLAN, J. CHAUMONT, R. MEUNIER and H. BERNAS, *Nucl. Instrum. Methods* B **45** (1990) 293.
9. J. J. JIA, T. A. CALLCOTT, J. YURKAS, A. W. ELLIS, F. J. HIMPSEL, M. G. SAMANT, J. STÖHR, D. L. EDERER, J. A. CARLISLE, E. A. HUDSON, L. J. TERMINELLO, D. K. SHUH and R. C. C. PERERA, *Rev. Sci. Instrum.* **66** (1995) 1394.
10. P. SKYTT, J. GUO, N. WASSDAHL, J. NORDGREN, Y. LUO and H. AGREN, *Phys. Rev.* A **52** (1995) 3572.
11. A. ST-AMANT and D. R. SALAHUB, *Chem. Phys. Lett.* **169** (1990) 387.
12. A. ST-AMANT, Ph. D. thesis, University of Montreal, 1991.
13. M. J. S. DEWAR and E. G. ZOEBISCH, *Theochem.* **180** (1988) 1; M. J. S. DEWAR, E. G. ZOEBISCH, E. F. HEALY and J. J. P. STEWART, *J. Am. Chem. Soc.* **107** (1985) 3902.
14. A. D. BECKE, *Phys. Rev.* A **38** (1988) 3098.
15. J. P. PERDEW, *ibid.* B **33** (1986) 8822.
16. S. N. SHAMIN, J. C. PIVIN and E. Z. KURMAEV, *J. Appl. Phys.* **73** (1993) 4605.
17. G. WIECH, H.-O. FELDHUTTER and A. SIMUNEK, *Phys. Rev.* B **47** (1993) 6981.
18. J.-J. YEH, "Atomic Calculation of Photoionization Cross Section and Asymetry Parameters" (Gordon and Breach Science, Langhorne, PA, 1993) p. 19047.